Multiple-viewpoint projection holograms synthesized by spatially incoherent correlation with broadband functions

Natan T. Shaked* and Joseph Rosen

Department of Electrical and Computer Engineering, Ben-Gurion University of the Negev, P.O. Box 653, Beer-Sheva 84105, Israel
**Corresponding author: natis@ee.bgu.ac.il*

Received February 7, 2008; revised June 17, 2008; accepted June 19, 2008; posted June 20, 2008 (Doc. ID 92530); published July 30, 2008

We present a theoretical framework for recording and reconstructing incoherent correlation holograms of real-existing three-dimensional scenes observed from multiple viewpoints. This framework is demonstrated by generating and reconstructing a modified Fresnel hologram as well as a new correlation hologram called a protected correlation hologram. The reconstructed scene obtained from the protected correlation hologram has a significantly improved transverse resolution for the far objects in the scene compared to the modified Fresnel hologram. Additionally, the three-dimensional information encoded into the protected correlation hologram is scrambled by a secretive point spread function and thus the hologram can be used for encrypting the observed scene. The proposed holography methods are demonstrated by both simulations and experiments. © 2008 Optical Society of America

OCIS codes: 090.1760, 090.1995, 100.6890, 110.6880.

1. INTRODUCTION

Since the work of Li *et al.* [1], several types of multiple-viewpoint projection (MVP) holograms have been proposed. The list includes Fourier holograms [1,2], Fresnel holograms [3,4], and Fresnel–Fourier holograms [4]. All these holograms are generated by first acquiring multiple projections of a three-dimensional (3D) scene from various viewpoints and then digitally processing the acquired projections to yield a digital hologram of the scene. In contrast to the composite hologram [5], the MVP hologram is equivalent to a single optical hologram of the same scene recorded from the central point of view. The recording process is performed by a regular digital camera and under an incoherent white light illumination, where no extreme stability of the optical system or powerful highly coherent laser source are required, as is usually necessary with conventional coherent holography techniques.

This study presents a theoretical framework for generating and reconstructing MVP holograms synthesized by spatial correlation between the 3D scene, incoherently illuminated, and broadband spatial functions. Figure 1 illustrates a possible optical system for acquiring the MVPs of the 3D scene. In this scheme the digital camera moves and acquires a different projection of the scene from each position. Instead of shifting the camera mechanically, we have also proposed the use of a microlens array for acquiring the entire viewpoint projections in a single camera shot [6]. Alternatively, one can acquire a small number of extreme projections simultaneously and predict the middle projections digitally by using the view synthesis algorithm [7]. Spatial multiplexing of several digital cameras is also possible.

Following the acquisition stage each projection is multiplied by the same two-dimensional (2D) broadband complex function (which should have a phase-only Fourier transform, as defined in Section 2), and the sum of the inner product is introduced into the corresponding pixel of the 2D hologram of the 3D scene. Alternatively, it is also possible to generate a one-dimensional (1D) hologram of the scene. In this case, each projection's row is multiplied by the same 1D broadband complex function and the column sum of all the inner products from each projection is introduced into the corresponding column in the hologram matrix. Since each projection is multiplied by the same spatial function, this process is actually a spatial correlation between the observed scene and a point spread function (PSF) and the resulting matrix is termed an incoherent correlation hologram. However, in contrast to other correlation holograms [8,9], the present holograms are produced from real-existing 3D objects illuminated by incoherent white light. The digital reconstruction of the incoherent correlation hologram is usually performed by convolving the hologram with the complex conjugate of the original generating PSF, scaled according to the reconstruction distance. Alternatively, the incoherent correlation hologram can be digitally converted to a known type of hologram (Fresnel, Fourier, etc), so that the 3D scene can also be optically reconstructed by illuminating the hologram with a coherent light. Another possibility is to reconstruct the hologram optically using an optical correlator [9].

The presented framework enables one to propose new types of digital holograms with certain advantages over the known holograms simply by choosing different PSFs. Recently [10], we have proposed a new incoherent correlation hologram called the digital incoherent modified

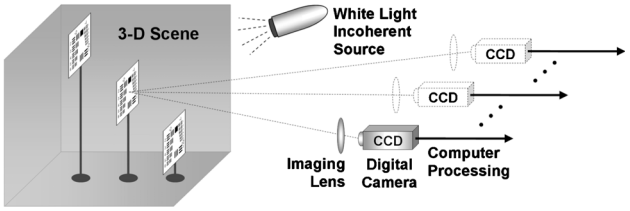

Fig. 1. Optical system for acquiring MVPs of the 3D scene along the horizontal axis.

Fresnel hologram (DIMFH), in which the 3D scene has been correlated with a PSF of a quadratic phase function. The DIMFH has been generated by processing the MVPs directly rather than by the previous indirect method [3,4], in which a Fourier hologram had been computed first, and only then was a Fresnel hologram generated from the reconstructed image of the first hologram. Therefore, redundant calculations and digital errors during the various transformations are avoided by using the DIMFH. Furthermore, this direct Fresnel holography method is not limited to small angles, in contrast to the MVP Fourier hologram and the indirect MVP Fresnel hologram, and hence the hologram reconstruction is more accurate.

In this study, by choosing a new broadband, space-limited, and secretive PSF, we also present a new incoherent correlation hologram called the digital incoherent protected correlation hologram (DIPCH). This hologram has a higher resolving power than the DIMFH, as well as the ability to encrypt the observed 3D information.

Following the presentation of the proposed framework in Section 2, we mathematically confirm its correctness in Section 3. Then, we show in Section 4 how to use this framework in order to propose two types of correlation holograms, the DIMFH and the DIPCH mentioned above. Sections 5 and 6 present simulation and experimental results, respectively, in which we demonstrate the generation and reconstruction of the DIMFH and the DIPCH and compare between them. Section 7 introduces some concluding remarks.

2. GENERATING AND RECONSTRUCTING INCOHERENT CORRELATION HOLOGRAMS

As mentioned above, by choosing different PSFs various types of incoherent correlation holograms can be generated from the acquired MVPs. For every hologram type, 1D or 2D holograms can be synthesized depending on the nature of the MVP aquisition. In case the MVPs are acquired only horizontally (as illustrated in Fig. 1) or along a different transverse axis, a 1D incoherent correlation hologram is generated. When the MVPs are acquired on a 2D grid of positions on the transverse plane, a 2D incoherent correlation hologram is generated. The 1D holograms are easier to produce because the projections are acquired along a single axis only. However, the 2D holograms have the advantage of encoding the 3D information into both axes. This advantage can be demonstrated with the following example. Assume that we record a 1D hologram of an object with the shape of a thin long horizontal line, where the camera moves along the long dimension of this line-shaped object. The axial location of the object is actually lost in the hologram and the reconstructed image is in focus along a long axial range. On the other hand, the 2D hologram contains the axial information, no matter what the recorded object shape is, and the image of the line-shaped object in the example above is in focus only in a single well-defined transverse plane, as it should be.

Next, we present the theory of generating and reconstructing 2D incoherent correlation holograms, where the theory of 1D incoherent correlation holograms (used in [10], for example) can be straightforwardly derived from the general 2D case.

The 2D incoherent correlation hologram is synthesized from $2K+1$ horizontal by $2K+1$ vertical projections of the 3D scene. We number the projections by m and n, so that the middle projection is denoted by $(m,n)=(0,0)$, the upper-right projection by $(m,n)=(K,K)$, and the lower-left projection by $(m,n)=(-K,-K)$. The (m,n)th projection $P_{m,n}(x_p,y_p)$ is multiplied by a PSF and the product is summed to the (m,n)th pixel in the following complex matrix:

$$H_2(m,n) = \int\int P_{m,n}(x_p,y_p)E_2(x_p,y_p)\mathrm{d}x_p\mathrm{d}y_p, \tag{1}$$

where $E_2(x_p,y_p)$ represents the generating PSF of the 2D hologram. This PSF is given by

$$E_2(x_p,y_p) = A_2(bx_p,by_p)\exp[ig_2(bx_p,by_p)], \tag{2}$$

where A_2 and g_2 are functions depending on (x_p,y_p) and may be chosen differently for each type of incoherent correlation hologram, and b is an adjustable parameter (with units that preserve the arguments of A_2 and g_2 as unitless quantities). Additionally, the function $E_2(x_p,y_p)$ has the property that its Fourier transform is a phase-only function. As we show in the following this condition is necessary to guarantee that the generated hologram can be reconstructed properly. The process manifested by Eq. (1) is repeated for all the projections, so that in the end of this digital process the resulting 2D complex matrix $H_2(m,n)$ represents the 2D incoherent correlation hologram of the 3D scene. The validation of this process is given in Section 3.

The reconstructed planar image $s_2(m,n;z_r)$, located at an axial distance z_r from the 2D hologram, is obtained by digitally convolving the hologram with the reconstructing PSF as follows:

$$s_2(m,n;z_r) = |H_2(m,n) * R_2(m,n;z_r)|, \tag{3}$$

where $*$ denotes a 2D convolution and $R_2(m,n;z_r)$ is the reconstructing PSF of the 2D hologram. This PSF is given by

$$R_2(m,n;z_r) = A_2\left(\frac{m\Delta p}{z_r},\frac{n\Delta p}{z_r}\right)\exp\left[-ig_2\left(\frac{m\Delta p}{z_r},\frac{n\Delta p}{z_r}\right)\right], \tag{4}$$

where A_2 and g_2 are the same functions used for the generating PSF of Eq. (2) and Δp is the pixel size of the digital camera.

Similar theory can also be applied for generating and reconstructing 1D incoherent correlation holograms [10].

However, in this case each row in the mth projection $P_m(x_p,y_p)$ is multiplied by the same 1D PSF $E_1(x_p)$ and the result is summed to the mth column in the 1D hologram $H_1(m,n)$. The reconstructed planar image $s_1(m,n;z_r)$, located at an axial distance z_r from the 1D hologram, is obtained by convolving the rows of the hologram matrix with the 1D reconstructing PSF $R_1(m;z_r)$.

3. MATHEMATICAL ANALYSIS OF THE DIGITAL PROCESS

This section provides verification that the reconstruction of the incoherent correlation hologram yields the image of the observed 3D scene. Here also, the analysis is carried out for the case of the 2D hologram, where the analysis of the 1D hologram is briefly discussed afterward. Therefore, contrary to what is illustrated in Fig. 1, we first assume that the MVPs of the 3D scene are acquired on a 2D grid. Figure 2 shows a top view of the optical system used for acquiring the MVPs. From this figure it is seen that the geometric relations between a point (x_s,y_s,z_s) at the 3D scene (where the coordinate origin is defined on the center of the imaging lens at the middle projection) and a point (x_p,y_p) on the (m,n)th projection $P_{m,n}(x_p,y_p)$ are given by

$$x_p = \frac{f(x_s - m\alpha)}{z_s}, \quad y_p = \frac{f(y_s - n\alpha)}{z_s}, \tag{5}$$

where f is the focal length of the imaging lens and α is the camera gap between two adjacent projections. Using Eqs. (5) the generating PSF, defined by Eq. (2), is

$$\begin{aligned} E_2(x_p,y_p) &= A_2(bx_p,by_p)\exp[ig_2(bx_p,by_p)] \\ &= A_2(\xi,\eta)\exp[ig_2(\xi,\eta)] = E_2(x_s - m\alpha, y_s - n\alpha; z_s), \end{aligned} \tag{6}$$

where

$$\xi = \frac{bf(x_s - m\alpha)}{z_s} = \frac{bf\alpha}{z_s\Delta p}\left(\frac{x_s\Delta p}{\alpha} - m\Delta p\right),$$

$$\eta = \frac{bf(y_s - n\alpha)}{z_s} = \frac{bf\alpha}{z_s\Delta p}\left(\frac{y_s\Delta p}{\alpha} - n\Delta p\right).$$

The complex distribution obtained on the hologram plane by a single source point, located in the 3D scene at coordinates (x_s,y_s,z_s), and having an infinitesimal size of $(\Delta x_s,\Delta y_s,\Delta z_s)$ and a value of $h(x_s,y_s,z_s)$, is given by

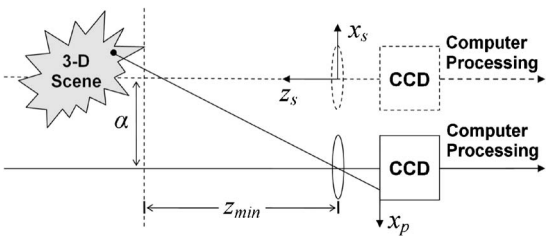

Fig. 2. Top view of the optical system of the MVP acquisition.

$$\begin{aligned} \tilde{H}_2(m,n;x_s,y_s,z_s) &= \int\int [h(x_s,y_s,z_s)\Delta x_s\Delta y_s\Delta z_s \\ &\quad \times \delta(x_p' - x_p, y_p' - y_p)]E_2(x_p',y_p')\mathrm{d}x_p'\mathrm{d}y_p' \\ &= h(x_s,y_s,z_s)E_2(x_p,y_p)\Delta x_s\Delta y_s\Delta z_s \\ &= h(x_s,y_s,z_s)E_2(x_s - m\alpha, y_s - n\alpha; z_s) \\ &\quad \times \Delta x_s\Delta y_s\Delta z_s. \end{aligned} \tag{7}$$

The overall distribution of the hologram, resulting from all the 3D scene points, is a volume integral over all the holograms of these single points as follows:

$$\begin{aligned} H_2(m,n) &= \int\int\int \tilde{H}_2(m,n;x_s,y_s,z_s)\mathrm{d}x_s\mathrm{d}y_s\mathrm{d}z_s \\ &= \int\int\int h(x_s,y_s,z_s)E_2(x_s - m\alpha, y_s - n\alpha; z_s)\mathrm{d}x_s\mathrm{d}y_s\mathrm{d}z_s. \end{aligned} \tag{8}$$

Equation (8) indeed indicates that for each value of z_s the hologram is a 2D correlation between the scene function $h(x_s,y_s,z_s)$ and the PSF.

To confirm that this hologram can be reconstructed to the image of the observed 3D scene, let us substitute the expression of the hologram [Eq. (8)] into Eq. (3) in order to obtain the reconstructed image $s_2(m,n;z_r)$ as follows:

$$\begin{aligned} s_2(m,n;z_r) &= |H_2(m,n) * R_2(m,n;z_r)| \\ &= \left|\int\int\left[\int\int\int h(x_s,y_s,z_s)E_2(x_s - m'\alpha, y_s - n'\alpha; z_s)\mathrm{d}x_s\mathrm{d}y_s\mathrm{d}z_s\right]R_2(m - m', n - n'; z_r)\mathrm{d}m'\mathrm{d}n'\right| \\ &= \left|\int\int\int h(x_s,y_s,z_s)\left[\int\int E_2(x_s - m'\alpha, y_s - n'\alpha; z_s)R_2(m - m', n - n'; z_r)\mathrm{d}m'\mathrm{d}n'\right]\mathrm{d}x_s\mathrm{d}y_s\mathrm{d}z_s\right| \\ &= \left|\int\int\int h(x_s,y_s,z_s)E_2(x_s - m\alpha, y_s - n\alpha; z_s) * R_2(m,n;z_r)\mathrm{d}x_s\mathrm{d}y_s\mathrm{d}z_s\right|. \end{aligned} \tag{9}$$

Let us define $\phi(\nu_m,\nu_n)$ so that $\mathrm{FT}\{E_2(m\Delta p,n\Delta p)\}=\exp[i\phi(\nu_m,\nu_n)]$, where FT denotes a Fourier transform. Since R_2 and E_2 are a complex conjugate pair, $\mathrm{FT}\{R_2(m\Delta p,n\Delta p)\}=\exp[-i\phi(-\nu_m,-\nu_n)]$. Using Eqs. (4) and (6) we first calculate the convolution between the generating and the reconstructing PSFs in Eq. (9) as the following:

$$\begin{aligned}E_2(x_s-m\alpha,y_s-n\alpha;z_s)*R_2(m,n;z_r)&=\mathrm{FT}^{-1}\{\mathrm{FT}\{E_2(x_s-m\alpha,y_s-n\alpha;z_s)\}\cdot\mathrm{FT}\{R_2(m,n;z_r)\}\}\\&=\mathrm{FT}^{-1}\left\{\mathrm{FT}\{A_2(\xi,\eta)\exp[ig_2(\xi,\eta)]\}\cdot\mathrm{FT}\left\{A_2\left(\frac{m\Delta p}{z_r},\frac{n\Delta p}{z_r}\right)\exp\left[-ig_2\left(\frac{m\Delta p}{z_r},\frac{n\Delta p}{z_r}\right)\right]\right\}\right\}\\&=C\cdot\mathrm{FT}^{-1}\left\{\exp\left[i\phi\left(\frac{-z_s\Delta p}{\alpha bf}\nu_m,\frac{-z_s\Delta p}{\alpha bf}\nu_n\right)\right]\exp\left[-i\left(\frac{x_s\Delta p}{\alpha}\nu_m+\frac{y_s\Delta p}{\alpha}\nu_n\right)\right]\right.\\&\quad\left.\cdot\exp[-i\phi(-z_r\nu_m,-z_r\nu_n)]\right\}\\&=C\cdot\delta\left(m\Delta p-\frac{x_s\Delta p}{\alpha},n\Delta p-\frac{y_s\Delta p}{\alpha};z_r-\frac{z_s\Delta p}{\alpha bf}\right),\end{aligned}\tag{10}$$

where FT^{-1} denotes an inverse Fourier transform and C is a constant. Thus, after substituting the result of Eq. (10) back into Eq. (9) the reconstruction image is

$$\begin{aligned}s_2(m,n;z_r)&=\left|C\cdot\int\int\int h(x_s,y_s,z_s)\delta\left(m\Delta p-\frac{x_s\Delta p}{\alpha},n\Delta p-\frac{y_s\Delta p}{\alpha};z_r-\frac{z_s\Delta p}{bf\alpha}\right)\mathrm{d}x_s\mathrm{d}y_s\mathrm{d}z_s\right|\\&=\left|C\cdot h\left(m\Delta p\cdot\frac{\alpha}{\Delta p},n\Delta p\cdot\frac{\alpha}{\Delta p};z_r\cdot\frac{bf\alpha}{\Delta p}\right)\right|.\end{aligned}\tag{11}$$

Equation (11) indicates that a scaled version of the 3D scene $h(x_s,y_s,z_s)$ is indeed reconstructed from the hologram and hence the correctness of the entire digital holographic process is verified. Note that under the condition that the Fourier transforms of the two PSFs, E_2 and R_2, are conjugate-pair phase-only functions, the convolution of Eq. (10) is equal to the delta function and consequently a proper reconstruction of the scene is obtained as shown in Eq. (11).

The transverse and the longitudinal magnifications of the proposed hologram resulting from Eq. (11) are

$$M_{2,x}=M_{2,y}=\frac{\Delta p}{\alpha},\quad M_{2,z}=\frac{\Delta p}{bf\alpha}.\tag{12}$$

Contrary to conventional MVP holograms, it is evident from Eqs. (12) that the magnifications of the proposed hologram are independent on the axial positions of the objects in the 3D scene. Therefore, the original scale relations between the various objects are maintained during the digital reconstruction, no matter whether the objects are close to or far from the acquisition plane. Hence, the digital image reconstructed from this hologram is a more accurate representation of the 3D scene. In addition, this special feature of the hologram may be very useful for optical 3D pattern recognition and object segmentation. Intuitively, this behavior can be explained as follows. Although farther objects look smaller than closer objects in each captured projection, they also "move" slower throughout the projections because of the parallax effect. The slower "movement" of farther objects broadens the correlation with the PSF in a way that the reduction of the image size in each projection is exactly compensated by the increment of the correlation size. However, if one still wants to eliminate this effect during the digital reconstruction process in order to obtain the perspective of a conventional optical imaging system, one should scale the reconstructed image by $M/M_{2,x}=(f/z_s)/(\Delta p/\alpha)=1/(bz_r)$ [since $z_r/z_s=\Delta p/(bf\alpha)$] for each and every reconstructed plane, where $M=f/z_s$ is the magnification of the imaging lens. This rescaling process is demonstrated in the results described in Section 5.

A similar mathematical confirmation can be applied for the 1D incoherent correlation hologram. In this 1D case, if the digital camera moves only horizontally (as shown in Fig. 1), the geometric relations between a point (x_s,y_s,z_s) at the 3D scene and a point (x_p,y_p) on the mth projection $P_m(x_p,y_p)$ are different from the 2D case and given by

$$x_p=\frac{f(x_s-m\alpha)}{z_s},\quad y_p=\frac{fy_s}{z_s}.\tag{13}$$

Following a similar mathematical analysis introduced for the 2D case, the reconstruction distribution in the 1D case is

$$s_1(m,n;z_r)=\left|C'\cdot h\left(m\Delta p\cdot\frac{\alpha}{\Delta p},n\Delta p\cdot\frac{z_s}{f};z_r\cdot\frac{bf\alpha}{\Delta p}\right)\right|,\tag{14}$$

where C' is a constant. Contrary to the 2D incoherent correlation hologram and based on Eq. (14), the magnifications of the 1D incoherent correlation hologram are

$$M_{1,x}=\frac{\Delta p}{\alpha},\quad M_{1,y}=\frac{f}{z_s},\quad M_{1,z}=\frac{\Delta p}{bf\alpha}.\tag{15}$$

Therefore, while the vertical magnification of the 1D hologram is dependent on the axial positions of the objects (as it is in conventional imaging systems), the horizontal magnification is constant (as it is in the 2D hologram). Hence, the aspect ratios of the reconstructed objects might be different from the aspect ratios of the original

observed objects. To eliminate this effect during the reconstruction process we can apply a scaling factor of $1/(bz_r)$ along the horizontal axis only. This rescaling process is demonstrated in the results presented in Section 6.

4. TWO EXAMPLES OF INCOHERENT CORRELATION HOLOGRAMS

In this section, we present two possible incoherent correlation holograms, the DIMFH and the DIPCH, where each has certain advantages over the other types of digital holograms. The only difference between the DIMFH and the DIPCH is the choice of the PSF used for generating each of the holograms. More types of incoherent correlation holograms might be found for gaining other advantages.

A. Digital Incoherent Modified Fresnel Hologram

The DIMFH is actually an incoherent Fresnel hologram generated directly by processing the MVPs of the 3D scene. However, since this hologram magnifies the various objects in the observed scene in a unique way, we call it a modified Fresnel hologram. This direct holography method is faster and more accurate than the Fourier-based Fresnel holography method [3,4], since redundant calculations and approximation errors are avoided. The generation and the reconstruction of the 1D DIMFH is performed by Eqs. (1) and (3) (but for the 1D case), respectively, where the generating PSF is a 1D quadratic phase function given by

$$E_1(x_p,y_p) = \exp(i2\pi b^2 x_p^2)\delta(y_p). \tag{16}$$

Similarly, the 2D DIMFH processing is carried out by Eqs. (1) and (3), where the generating PSF is a 2D quadratic phase function given by

$$E_2(x_p,y_p) = \exp[i2\pi b^2(x_p^2+y_p^2)]. \tag{17}$$

B. Digital Incoherent Protected Correlation Hologram

The DIPCH is a new incoherent correlation hologram that has two advantages over the Fresnel hologram in general and over the DIMFH in particular. First, since a random-constrained PSF is used to generate the hologram, only an authorized user that knows this PSF can reconstruct the 3D scene encoded into the hologram. By the term "random-constrained" we mean that this PSF is computed by an iterative algorithm initiated by a random function. Therefore, the DIPCH can be used as a method of encrypting the observed scene. Second, the reconstruction obtained from the DIPCH has a significantly higher transverse resolution for the far objects in the 3D scene compared to the DIMFH.

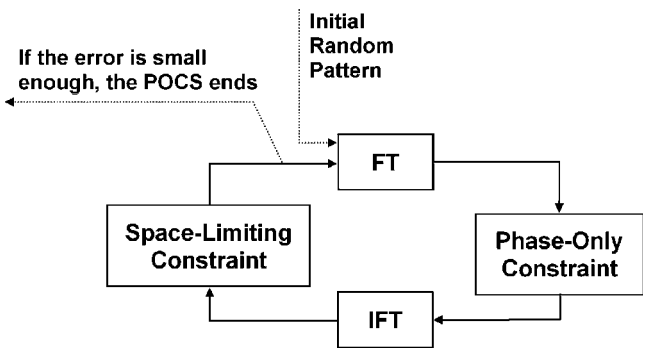

Fig. 3. Schematics of the POCS algorithm for finding the PSF of the DIPCH.

The DIPCH processing is still carried out by Eqs. (1) and (3). However, this time, the generating PSF is a space-limited random-constrained function that fulfills the constraint that its Fourier transform is a phase-only function. To find this PSF we use the projection onto constraint sets (POCS) algorithm [11,12]. The POCS algorithm used for finding this PSF is illustrated in Fig. 3. The POCS is an iterative algorithm that bounces from the PSF domain to its spatial spectrum domain and backward, using Fourier transform and inverse Fourier transform, respectively. In each domain the function is projected onto the constraint set. The two constraints of the POCS express the two properties required for the PSF of the DIPCH. First, the Fourier transform of the PSF should be a phase-only function. This requirement enables one to reconstruct the scene well from the DIPCH as provided by Eq. (10). Therefore, the constraint of the POCS in the spectral domain is the set of all phase-only functions and the Fourier transform of the PSF is projected onto this constraint by setting its magnitude distribution to the constant 1. The other property of the PSF is that it should be space limited into a relatively narrow region close to, but outside of, the origin. This condition reduces the reconstruction noise from the out-of-focus objects because the overlap during the convolution between the hologram at out-of-focus regions and the resampled space-limited reconstructing PSF is lower than in the case of using a widespread PSF. Of course, this noise is lower as much as the existence region of the PSF is narrower. However narrowing the existence region makes it difficult for the POCS algorithm to converge to a PSF that satisfies both constraints with an acceptable error. In any event, the constraint set in the PSF domain is all the complex functions that identically equal to zero in any pixel outside the predefined narrow existence region. Therefore, the projection onto the constraint set in the PSF domain is performed by multiplying the PSF by a function that is equal to one inside the narrow existence region of the PSF and zero elsewhere. In the case of the 1D DIPCH the constrained PSF is limited into a narrow strip of columns, whereas in the case of the 2D DIPCH the PSF is limited into a narrow ring. At the end of the process, the POCS algorithm yields the suitable random-constrained PSF that can be used in the hologram generation process. Figures 4(a) and 4(b) show the resulting phase distributions of the PSFs that were used for generating the 1D and the 2D DIPCHs, respectively.

In the following, we show that in the DIPCH the reconstruction resolution is improved compared to the DIMFH. In fact, far objects captured by the DIMFH are reconstructed with a reduced resolution for two reasons. (a) Due to the parallax effect, farther objects move slower throughout the projections, and therefore they sample a magnified version of the generating PSF. This magnified version has narrower bandwidth, and thus the recon-

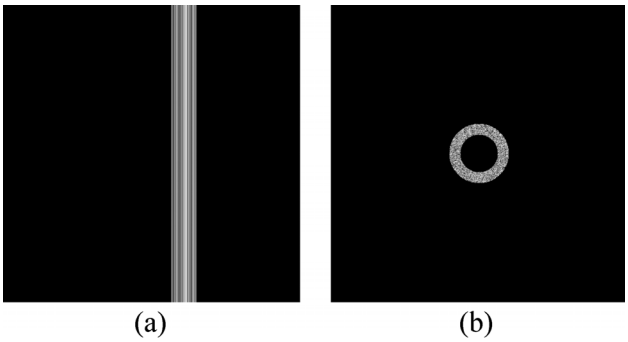

Fig. 4. Examples of the phase distributions of the generating random-constrained PSFs of (a) a 1D DIPCH and (b) a 2D DIPCH.

struction resolution of farther objects decreases. (b) The quadratic phase function used in the DIMFH has lower frequencies as one approaches its origin. Since far objects are correlated with the central part of the quadratic phase function along a range that becomes shorter as the object is farther, the bandwidth of the DIMFH of far objects becomes even narrower beyond the bandwidth reduction mentioned in (a). Contrary to the DIMFH, the spatial frequencies of the DIPCH's PSF are distributed uniformly all over its area. Therefore, the DIPCH sustains resolution reduction of far objects only due to reason (a). Hence, the images of far objects reconstructed from the DIPCH, besides being protected by the random-constrained PSF, also have higher resolution.

Let us show quantitatively that the resolution of far objects reconstructed from the DIMFH is worse than that of the DIPCH. The bandwidth of the generating PSF is determined by the movement (throughout the projections) of the object point that is the closest to the imaging lens. For a distance of α between any two consecutive projections and for a distance of $z_{\min}$ between the closest object point and the imaging lens, the smallest shift that can be recorded on the camera is $\alpha f/z_{\min}$, where $f/z_{\min}$ is the maximal magnification of the imaging lens. $\alpha f/z_{\min}$ is also the minimal practical feature size of the generating PSF because a smaller feature size cannot be detected by the camera due to the minimal sampling gap of $\alpha f/z_{\min}$. For this reason, the smallest object detail that can be recorded and reconstructed by the DIPCH is $\alpha f/(Mz_{\min})$. Recalling that $M=f/z_s$, one realizes that the DIPCH's reconstruction resolution linearly decreases for the far objects in the 3D scene.

For a single object point, the resulting hologram in the case of the DIMFH is exactly the PSF given by Eq. (16) or (17). These expressions are actually equal to the transfer function of a lens for which the resolution properties are well known. For a single point located at distance $z_{\min}$ from the imaging system, the width of the recorded hologram is $2K\alpha f/z_{\min}$ and the smallest resolved detail is $\alpha f/(Mz_{\min})$. Now, for a point located at distance z_s from the imaging system, the width of the recorded hologram is $2K\alpha f/z_s$. Since, as explained above, the DIMFH of an object point located at distance z_s from the imaging system is equivalent to a lens, the hologram resolving power is linearly dependent on its width. Thus, the resolved detail of an object at distance z_s is the smallest-ever resolved detail $\alpha f/(Mz_{\min})$ multiplied by the ratio of the maximum hologram width, $2K\alpha f/z_{\min}$, and the actual hologram width, $2K\alpha f/z_s$. Hence, the resolved detail of an object at a certain distance z_s is $\alpha f z_s/(Mz_{\min}^2)$ in the case of DIMFH. We recall that the size of the resolved detail in the case of the DIPCH is $\alpha f/(Mz_{\min})$. Therefore, the ratio of the minimum resolved detail of the DIMFH and the DIPCH is $z_s/z_{\min}$. This means that the farther the object from the imaging lens is, the worse the resolving power of the DIMFH, compared to the DIPCH, becomes. In Sections 5 and 6 we demonstrate this conclusion by simulations and experiments.

5. SIMULATION RESULTS

To demonstrate the generation of 2D correlation holograms by simulation we first generated the 3D scene projections in the computer. The 3D scene was composed of three equal-size partial United States Air Force (USAF) resolution charts positioned at different transverse and axial locations relative to the camera. To simulate this situation the chart sizes on each computer-generated projection plane were determined according to their axial positions from the plane, where farther charts appeared smaller than closer charts. In addition, the charts were positioned at different transverse locations in each computer-generated projection, where closer charts moved faster than farther charts throughout the different projections. Figure 5 shows the eight most extreme, and the central projections, out of the 600×600 projections synthesized in the computer as the input for the hologram generation algorithms. Note that we synthesized these projections with partial object occlusions in part of the projections to demonstrate that the method is resistant against these occlusions.

For comparison purposes we generated both a 2D DIMFH and a 2D DIPCH. As described by Eqs. (1) and (17) to generate the 2D DIMFH we multiplied each projection by a 2D quadratic phase function and then summed each of the inner products to the corresponding pixel in the hologram. Figure 6(a) presents the magnitude and phase of the 2D DIMFH generated by this process. As described by Eqs. (2)–(4) and (17), reconstructing the 3D scene from this hologram digitally was carried out by convolving the hologram with 2D quadratic phase functions with a phase sign opposite to the generating PSF. The three 2D quadratic phase functions yielding the best in-focus reconstructed planes are shown in Fig. 6(b). The corresponding reconstructed planes are shown in Fig. 6(c). In each plane only a single USAF resolution chart is in focus, whereas the other two charts are out of focus. This holographic phenomenon validates that the volume information is indeed encoded into the hologram. As explained in Section 3, a 2D resampling process should be performed on the reconstructed planes to retain the original depth perspective of far and close objects in the 3D scene. These rescaled, best in-focus, reconstructed planes are shown in Fig. 6(d). Figure 6(e) presents zoomed-in images of the best in-focus USAF resolution charts shown in Fig. 6(d). Evidently from these figures, the resolution of the reconstructed charts decreases as the distance of the objects from the acquisition plane increases.

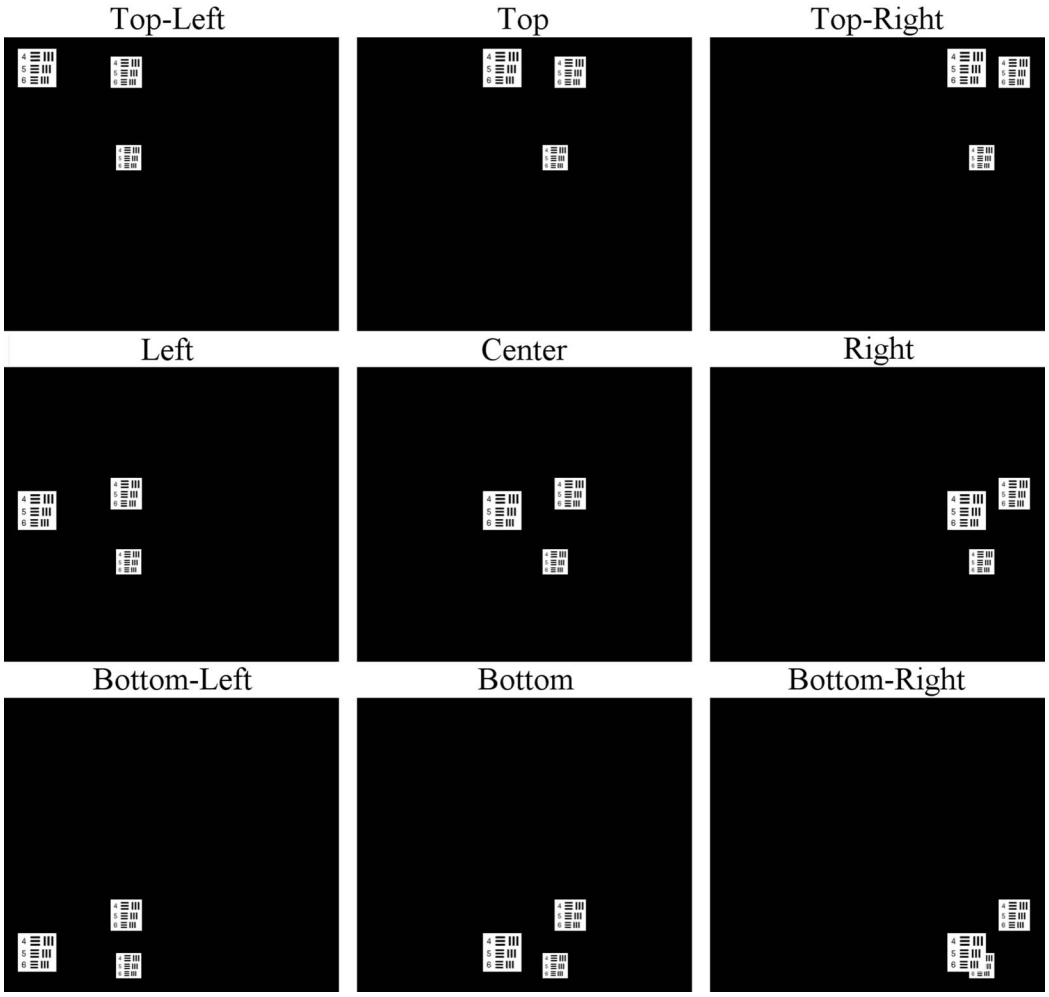

Fig. 5. Several projections taken from the entire computer-generated set containing 600×600 projections, used for generating the 2D DIMFH and the 2D DIPCH.

The same computer-generated projections were used for generating the 2D DIPCH. For this purpose, each projection was multiplied by the PSF of Fig. 4(b), computed by the POCS algorithm. The inner product between each projection and the PSF was summed to a single complex value, which was introduced into the corresponding pixel in the 2D DIPCH. The magnitude and the phase of the resulting 2D hologram are shown in Fig. 7(a). The reconstruction from this hologram was obtained by convolving it with the conjugate function of the generating PSF scaled differently in order to reconstruct a different transverse plane with each scaled PSF. The phases of the three PSFs that yield the best in-focus reconstructed planes and the corresponding best in-focus reconstructed planes are shown in Figs. 7(b) and 7(c), respectively. Here again, the fact that in each of the reconstructed planes one USAF resolution chart is in focus whereas the other two charts are out of focus demonstrates that the 3D information is encoded properly into this hologram. Then again, we performed a 2D resampling process on the reconstructed planes for retaining the original depth perspective. The resampled best in-focus reconstructed planes are shown in Fig. 7(d). Figure 7(e) shows zoomed-in images of the best in-focus USAF resolution chart in each of these resampled reconstructed planes. Comparing between the best in-focus reconstructed charts obtained from the DIPCH [Fig. 7(e)] and from the DIMFH [Fig. 6(e)], one realizes that the far objects reconstructed from the DIPCH have a significantly better resolution than those reconstructed from the DIMFH, although the former are a bit noisier due to the nonuniformity of the gray levels of the random-constrained PSF generated by the POCS algorithm.

6. EXPERIMENTAL RESULTS

The experiment of synthesizing 1D incoherent correlation holograms was carried out on the optical system illustrated in Fig. 1. Three equal-size USAF resolution charts, 8.5 cm×8.5 cm each, were positioned at the 3D scene in front of a dark background and were illuminated by a halogen white light. The axial distance between the first and the second charts, as well as between the second and the third charts, was 10 cm. The distance between the closest chart and the camera was 50 cm. The digital camera (CCD type, model: PCO, Scientific 230XS, containing 1280×1024 pixels and an 8.6 mm×6.9 mm active area) was positioned on a micrometer slider and captured 1200 projections of the 3D scene across a horizontal range of 24 cm. Note that in contrast to the 2D hologram, in which

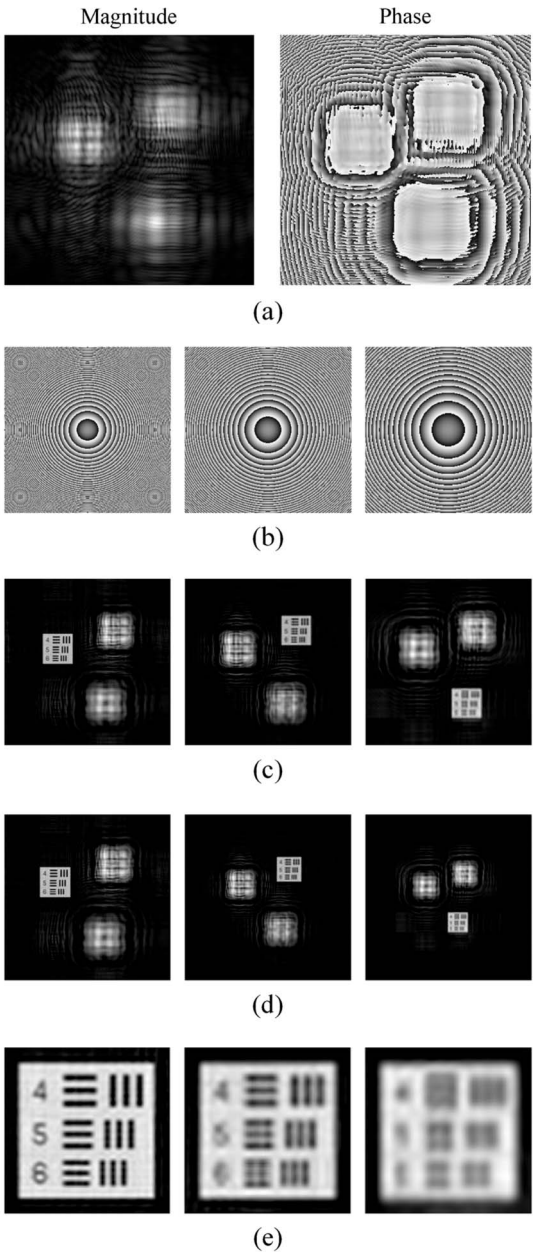

Fig. 6. Generating and reconstructing the 2D DIMFH: (a) magnitude and phase of the hologram; (b) the phase distributions of the reconstructing PSFs used for obtaining the three best in-focus reconstructed planes; (c) the corresponding three best in-focus reconstructed planes along the optical axis; (d) same as (c), but after the 2D resampling process; (e) zoomed-in images of the corresponding best in-focus reconstructed objects.

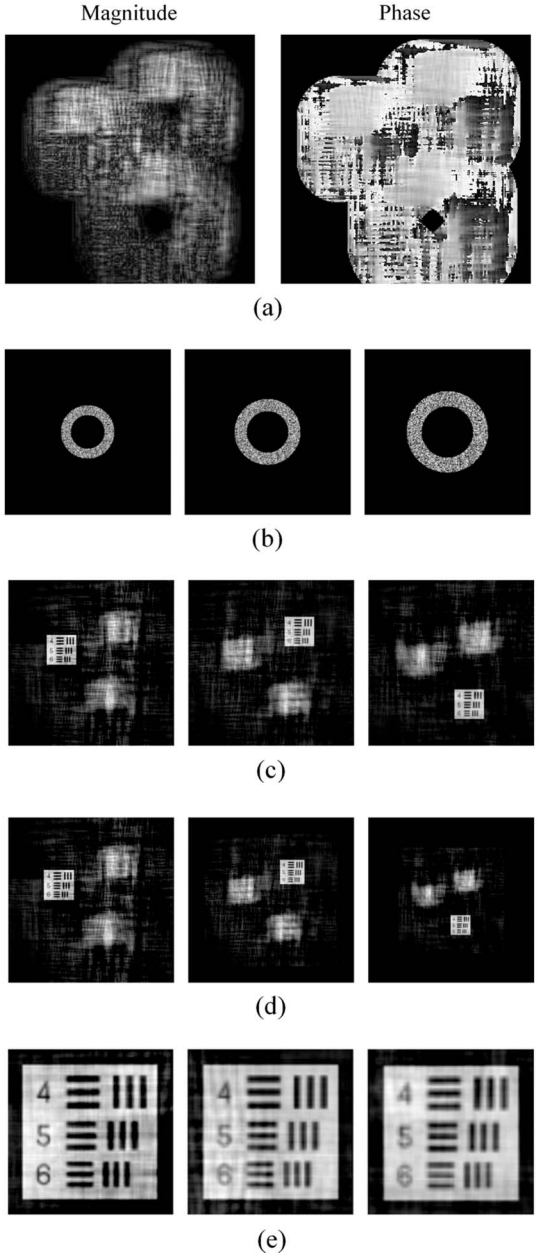

Fig. 7. Generating and reconstructing the 2D DIPCH: (a) magnitude and phase of the hologram; (b) the phase distributions of the reconstructing PSFs used for obtaining the three best in-focus reconstructed planes; (c) the corresponding three best in-focus reconstructed planes along the optical axis; (d) same as (c), but after the 2D resampling process; (e) zoomed-in images of the corresponding best in-focus reconstructed objects.

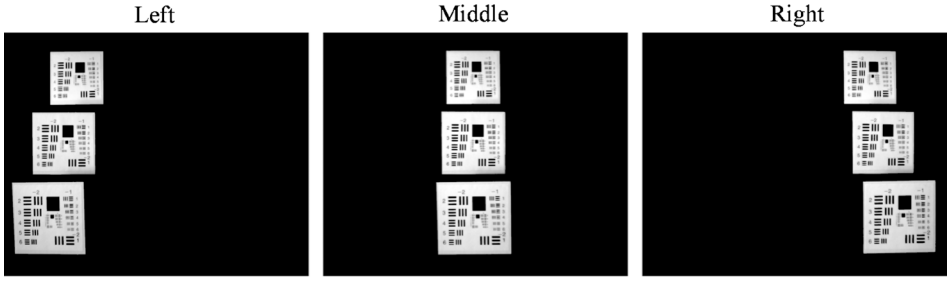

Fig. 8. Several projections taken from the entire experimentally obtained set containing 1200 projections, used for generating the 1D DIMFH and the 1D DIPCH.

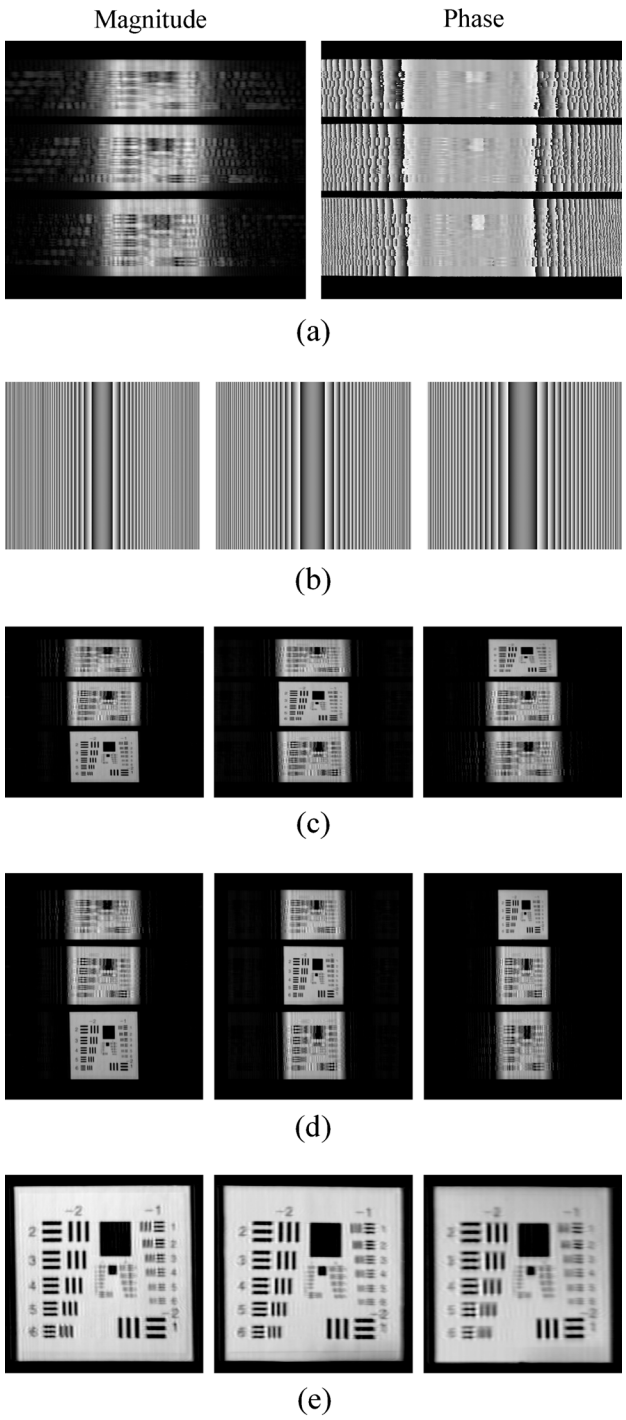

Fig. 9. Generating and reconstructing the 1D DIMFH: (a) magnitude and phase of the hologram; (b) the phase distributions of the reconstructing PSFs used for obtaining the three best in-focus reconstructed planes; (c) the corresponding three best in-focus reconstructed planes along the optical axis; (d) same as (c), but after the 1D resampling process; (e) zoomed-in images of the corresponding best in-focus reconstructed objects.

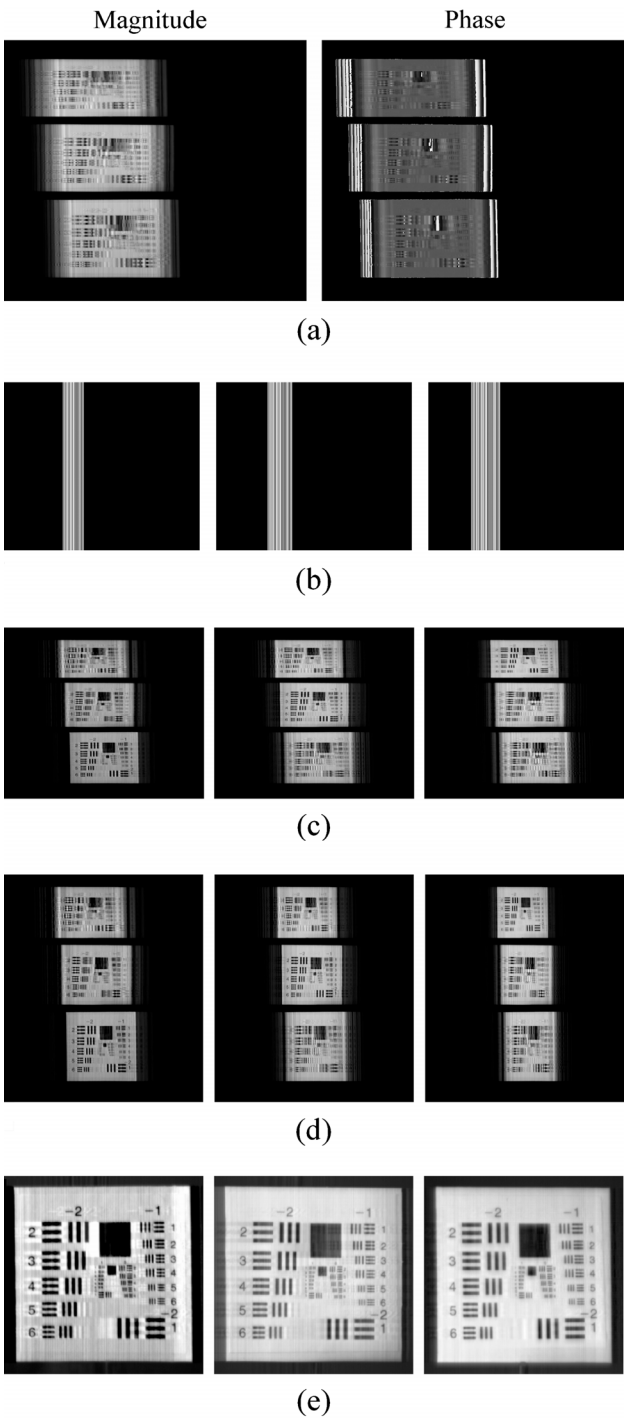

Fig. 10. Generating and reconstructing the 1D DIPCH: (a) magnitude and phase of the hologram; (b) the phase distributions of the reconstructing PSFs used for obtaining the three best in-focus reconstructed planes; (c) the corresponding three best in-focus reconstructed planes along the optical axis; (d) same as (c), but after the 1D resampling process; (e) zoomed-in images of the corresponding best in-focus reconstructed objects

the projections of the 3D scene have to be acquired on a 2D grid, in the 1D hologram the camera moves along a single axis only. Figure 8 shows the two most extreme and the central projections taken from the entire set of 1200 projections.

These captured projections were used in order to generate both the 1D DIMFH and the 1D DIPCH. The 1D DIMFH was generated, according to Eqs. (1), (2), and (16), by multiplying each projection by a 1D quadratic phase function and summing the inner product to the corresponding column in the 1D DIMFH. The amplitude and phase of the resulting hologram are shown in Fig. 9(a). According to Eqs. (2)–(4) and (16) the reconstruction from this 1D DIMFH was obtained by a 1D convolution of the

hologram with 1D quadratic phase functions in which the phase sign is opposite to the generating PSF. The three best in-focus reconstructing PSFs and the corresponding best in-focus reconstructed planes are shown in Figs. 9(b) and 9(c), respectively. In each of the planes shown in Fig. 9(c) a different USAF resolution chart is in focus, whereas the other two charts are out of focus. This validates the success of the holographic process of the 1D DIMFH. As explained in Section 3, resampling these reconstructed planes along the horizontal axis is required in order to retain the original aspect ratios of the objects. These resampled best in-focus reconstructed planes are shown in Fig. 9(d). Looking on the corresponding zoomed-in images of the best in-focus charts, shown in Fig. 9(e), one can conclude that the far objects in the 3D scene indeed have a reduced horizontal resolution compared to the close objects in the scene, due to the reasons explained in Subsection 4.B.

A 1D DIPCH was generated by multiplying each of the acquired projections by the random-constrained PSF of Fig. 4(a), computed for the 1D case by the POCS algorithm. Next, each inner product was summed to a single column in the 1D DIPCH, the amplitude and phase of which are shown in Fig. 10(a). To reconstruct the 3D scene from this hologram the DIPCH was convolved with the conjugate of a scaled version of the same PSF used for the hologram generation. The phases of the three reconstructing PSFs, yielding the best in-focus reconstructed planes, are shown in Fig. 10(b). The corresponding reconstructed planes are shown in Fig. 10(c). As before, in each of these planes a different USAF chart is in focus, whereas the other two charts are out of focus. Once again, a resamapling process was applied on the horizontal axis of the reconstructed planes for retaining the original aspect ratios of the objects. Figure 10(d) shows these resampled best in-focus reconstructed planes, whereas Fig. 10(e) shows the corresponding zoomed-in images of the best in-focus charts at these three planes. As in the 2D case farther objects have a higher resolution (horizontal resolution for the 1D case) in the DIPCH [Fig. 10(e)] compared to the DIMFH [Fig. 9(e)]. Once again, this property signifies the advantage of the DIPCH over the DIMFH, where the other advantage of the DIPCH is being protected by the random-constrained PSF used for generating the hologram.

7. CONCLUSIONS

We have presented a theoretical framework for generating and reconstructing 1D and 2D incoherent correlation holograms. These holograms are synthesized from MVPs of a 3D scene illuminated by incoherent white light, without the need for special laboratory conditions. A proper digital process, involving multiplication of each of the MVPs by a certain broadband PSF and summation of each of the products, yields the final incoherent correlation hologram of the 3D scene. Different PSFs generate different types of holograms. Two examples have been presented: (a) the DIMFH, which is an incoherent Fresnel hologram generated directly, without approximations or redundant calculations; and (b) the DIPCH, which enables one to encode the 3D scene in a secured way and to image the scene with a significantly improved resolution. These new holograms have been demonstrated by both simulation and experiments. In the future, the proposed framework might be used to find new types of incoherent correlation holograms for other purposes and with other advantages over the existing types of holograms.

REFERENCES

1. Y. Li, D. Abookasis, and J. Rosen, "Computer-generated holograms of three-dimensional realistic objects recorded without wave interference," Appl. Opt. **40**, 2864–2870 (2001).
2. D. Abookasis and J. Rosen, "Computer-generated holograms of three-dimensional objects synthesized from their multiple angular viewpoints," J. Opt. Soc. Am. A **20**, 1537–1545 (2003).
3. Y. Sando, M. Itoh, and T. Yatagai, "Holographic three-dimensional display synthesized from three-dimensional Fourier spectra of real existing objects," Opt. Lett. **28**, 2518–2520 (2003).
4. D. Abookasis and J. Rosen, "Three types of computer-generated hologram synthesized from multiple angular viewpoints of a three-dimensional scene," Appl. Opt. **45**, 6533–6538 (2006).
5. T. Yatagai, "Stereoscopic approach to 3-D display using computer-generated holograms," Appl. Opt. **15**, 2722–2729 (1976).
6. N. T. Shaked, J. Rosen, and A. Stern, "Integral holography: white-light single-shot hologram acquisition," Opt. Express **15**, 5754–5760 (2007).
7. N. T. Shaked, B. Katz, and J. Rosen, "Fluorescence multicolor hologram recorded by using a macrolens array," Opt. Lett. **33**, 1461–1463 (2008).
8. B. Javidi and A. Sergent, "Fully phase encoded key and biometrics for security verification," Opt. Eng. **36**, 935–942 (1997).
9. D. Abookasis and J. Rosen, "Digital correlation holograms implemented on a joint transform correlator," Opt. Commun. **225**, 31–37 (2003).
10. N. T. Shaked and J. Rosen, "Modified Fresnel computer-generated hologram directly recorded by multiple-viewpoint projections," Appl. Opt. **47**, D21–D27 (2008).
11. J. R. Fienup, "Phase retrieval algorithms: a comparison," Appl. Opt. **21**, 2758–2769 (1982).
12. H. Stark, ed., *Image Recovery: Theory and Application* (Academic, 1987), pp. 29–78 and 277–320.